

INFRARED ECHO AND LATE-STAGE REBRIGHTENING OF NUCLEAR TRANSIENT PS1-10ADI: EXPLORING TORUS BY TIDAL DISRUPTION EVENT IN ACTIVE GALACTIC NUCLEI

NING JIANG^{1,2}, TINGGUI WANG^{1,2}, GUOBIN MOU³, HUI LIU^{1,2}, LIMING DOU⁴, ZHENFENG SHENG^{1,2}, YIBO WANG^{1,2}

Draft version December 5, 2018

ABSTRACT

Tidal disruption events (TDEs) in active galactic nuclei (AGNs) have been overlooked for a long time but tentatively been investigated recently. We report the discovery of a long-lasting luminous mid-infrared (mid-IR) flare in PS1-10adi, which is a newly-identified highly energetic transient event occurred in AGN. The IR luminosity of PS1-10adi, as well as other analogous events, are at least one order of magnitude higher than all known supernova, but can be well interpreted as the dust echoes of TDEs, whose ultra-high IR energy is reprocessed from the dusty torus around the black hole. The torus dust is sublimating during the early stage of the outburst and probably lead to the observed rapid emergence of Fe II lines. Moreover, the UV-optical rebrightening and contemporaneous X-ray onset after ~ 1500 rest-frame days since the optical peak is also an intriguing feature of PS1-10adi, which could be attributed to the interaction between the high-velocity outflow and torus. We suggest that the luminous IR echo is a very typical phenomenon of TDEs in AGNs and may provide us an ideal opportunity to explore the torus properties.

Subject headings: galaxies: individual (PS1-10adi) — galaxies: active — galaxies: nuclei — infrared:galaxies

1. INTRODUCTION

The stellar or gas kinematics on nearby galaxies in the past two decades have established that supermassive black holes (SMBHs), with masses of $10^6\text{--}10^8 M_\odot$, are universal in the centers of galaxies with massive bulges. Furthermore, the tight correlations between the BH mass (M_{BH}) and various bulge properties indicate an attractive co-evolutionary growth of SMBHs and their host galaxies (see reviews by Kormendy & Ho 2013 and Heckman & Best 2014). The widespread picture is not unquestionable but still competed by some alternative views which claim that their relation can emerge as the result of a statistical convergence process without a physical coupling (e.g., Peng 2007; Jahnke & Macciò 2011) or the dark matter might be influential (e.g., Ostriker 2000; Zhao et al. 2002; Bogdán & Goulding 2015). Whatever, SMBHs are normally believed to accumulate their mass through the phase of active galactic nuclei (AGN), during which the BHs are efficiently accreting surrounding materials. AGNs themselves are also the best evidence of the existence of SMBHs in distant galaxies, which are otherwise beyond the current capabilities for direct dynamical measurement.

Nevertheless, the detection of SMBHs in normal galaxies are still very difficult provided that vast majority of them are quiescent and faraway. Although some new approaches seem promising to detect SMBHs at cosmological distances, such as gravitational lensing (e.g., Mao et al. 2001; Hezaveh et al. 2015; Chen et al. 2018) and future gravitational wave observations of SMBH mergers or the inspiral of compact stellar remnants consumed by SMBH, they are not so efficient and practical for the time being. Heaven will always leave a door

open, the so-called tidal disruption event (TDE) could offer us the greatest chance to catch sight of these dormant SMBHs. The TDE happens if a star in the galaxy wanders too close to the central black hole, the star can be ripped apart when the tidal force exceeds its self-gravity and roughly half mass of the star will be accreted on to the black hole while the remaining half may be ejected by the simple classical theory (Rees 1988). Recent works reveal that the real accreting fraction could be much lower since most of the mass may join in an outflow (e.g., Metzger & Stone 2016). A luminous flare of electromagnetic radiation is expected during this process with emission peaks in the UV or soft X-rays and a characteristic $t^{-5/3}$ decline on timescale of months to years (Rees 1988; Phinney 1989). The TDE event rate is estimated to be 10^{-4} to 10^{-5} galaxy⁻¹yr⁻¹ and might be highest in nucleated dwarf galaxies (Wang & Merritt 2004, Stone & Metzger 2016).

Observationally, TDEs are though first discovered in X-ray bands serendipitously, the field has not experienced explosive growth until the past decade, benefited from a batch of dedicated optical time-domain surveys (see Komossa 2015 as a review). To avoid any potential contaminations stemmed from variability of AGN, traditional searching of TDEs care about solely normal galaxies and neglected active galaxies (e.g., van Velzen et al. 2011). However, TDEs might also occur in AGNs and the rates are expected to be even high (Karas & Šubr 2007), not to mention that TDEs were actually first proposed out as a possible power source of AGNs and quasars (Hills 1975). Recently, Blanchard et al. 2017 have claimed a TDE candidate PS16dtm found in the Panoramic Survey Telescope and Rapid Response System (Pan-STARRS). This event occurs in a Seyfert 1 galaxy with $M_{\text{BH}} \sim 10^6 M_\odot$, and display some distinctive features, such as a plateau phase, disappeared prior X-ray emission and newly-emerging strong Fe II emission. Soon thereafter, Kankare et al. (2017, hereafter K17) have reported the other high energetic Pan-STARRS transient event named PS1-10adi with a total radiated energy of $\sim 2.3 \times 10^{52}$ erg. The rapid smooth brightening light curve and persistently narrow spectral lines over ~ 3 yr of PS1-10adi is inconsistent with known types of

¹ Key laboratory for Research in Galaxies and Cosmology, Department of Astronomy, University of Science and Technology of China, Chinese Academy of Sciences, Hefei, Anhui 230026, China; jnac@ustc.edu.cn

² School of Astronomy and Space Sciences, University of Science and Technology of China, Hefei, Anhui 230026, China

³ School of Physics and Technology, Wuhan University, Wuhan 430072, China

⁴ Center for Astrophysics, Guangzhou University, Guangzhou 510006, China

recurring BH variability, yet may be linked to a TDE or super-nova (SNe) in the nuclear region powered by shock interaction between expanding material and large quantities of surrounding dense matter. K17 have even unveiled possibly a population of such kind of events in the centers of active galaxies yet to be further explored.

Encouraged by our successful detection of a mid-infrared (mid-IR) flare in PS16dtm and valuable implications learned from it (Jiang et al. 2017), we have also checked the mid-IR variability of PS1-10adi and discovered a long-lasting flare not surprisingly in the location coincident with PS1-10adi using data from the *Wide-field Infrared Survey Explorer* (*WISE*; Wright et al. 2010; Mainzer et al. 2014). In addition, we have noticed an odd late-stage rebrightening in the UV-optical light curve as well as a corresponding mid-IR signal. The mid-IR emission in radio-quiet AGNs is generally thought to be associated with thermal emission from dust at parsec-scale distances from the central SMBH. On the other hand, an optically thick obscuring medium in the equatorial plane (commonly dubbed the "torus") is needed in the unified model, the current paradigm suggests that the IR-emitting dust is the same medium as the obscuring material. This is reflected by the widespread use of torus models in order to reproduce IR spectral energy distributions (SEDs, see a recent review on torus in Netzer 2015. Basing on the fact of a pre-existing dusty torus, mid-IR echoes are predictable for those TDEs in active galaxies, which would expose the torus itself dynamically. The ubiquitous luminous IR echoes associated with TDEs in AGNs may be one of the most notable characteristics distinguished from SNe (see §5).

In this paper, we will try to analyze all of these new recognized phenomenons in PS1-10adi and understand them under the context of TDEs in AGNs. We assume a cosmology with $H_0 = 70 \text{ km s}^{-1} \text{ Mpc}^{-1}$, $\Omega_m = 0.3$, and $\Omega_\Lambda = 0.7$. At a redshift of $z = 0.203$, PS1-10adi has a luminosity distance of 996.5 Mpc.

2. MID-IR LIGHT CURVES

The *WISE* has performed a full-sky imaging survey in four broad mid-IR bandpass filters centered at 3.4, 4.6, 12 and $22 \mu\text{m}$ (labeled W1-W4) from 2010 February to August. The solid hydrogen cryogen used to cool the W3 and W4 instrumentation was depleted later and it was placed in hibernation in 2011 February. *WISE* was reactivated and renamed *NEOWISE-R* since 2013 October, using only W1 and W2, to hunt for asteroids that could pose as impact hazard to the Earth. *WISE* has scanned a specific sky area every half year and thus yielded 10-11 times of observations for every object up to now. For each epoch, there are 10-20 single exposures. We use only the best quality single frame images by selecting only detections with data quality flag 'qual_frame' > 0.

PS1-10adi is a point-like source in *WISE* images without any potential contamination within $10''$. We have collected all of its public *WISE* photometric data, including from ALLWISE and *NEOWISE-R* catalogs. The data are distributed in 10 epochs at intervals of about six months from 2010 May 9 (MJD=55,325) up to 2017 Oct 22 (MJD=58,048). The light curves in W1 and W2 are presented in Figure 1. For ease of comparison, its optical light curve (*V*-band) has also been overplotted. First, no reliable variability is detected within each epoch and thus we then average these data to obtain a mean value at each epoch following our previous works (Jiang et al. 2012; 2016). We noticed that the first *WISE* epoch ("E1") is 98 days earlier and the second epoch ("E2") is 82

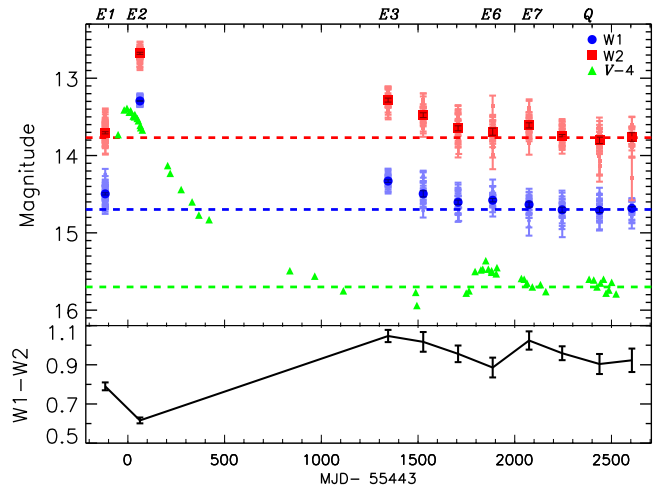


FIG. 1.— The *WISE* W1 ($3.4 \mu\text{m}$, blue squares) and W2 ($4.6 \mu\text{m}$, red triangles) light curves of PS1-10adi. The horizontal dashed lines represent the background magnitudes estimated from the latest three epochs. The *V*-band light curve is also plotted for comparison (green triangles). The W1-W2 color is shown in the bottom panel.

days after the optical discovery date, or -117 (rest-frame -97) days and 63 (52) days since the optical peak. PS1-10adi has began brightened by ~ 1 mag in W1 and W2 at E2 relative to E1. Unfortunately the *WISE* went into hibernation soon and hasn't yielded the third observation until 2014 May, resulting in a gap of 1282 days between E2 and E3. The light curve presents a declining trend at E3 and thereafter and keeps at a constant level in the near past. In order to isolate the host galaxy and AGN emission (or background emission as a whole) from the outburst phase, We take the last three epochs as the quiescent state, which contributes an averaged magnitude of 14.70 ± 0.02 and 13.77 ± 0.03 at W1 and W2, respectively. The original and background-subtracted magnitudes are shown in Table 1. It's interesting to note that PS1-10adi is already brighter at E1, by 0.20 ± 0.02 and 0.06 ± 0.03 magnitudes in W1 and W2, respectively. The W1-W2 color has generally been used as a rough assessment of the AGN or stellar dominance of a galaxy, for instance, $W1-W2 > 0.8$ for AGN-like or $W1-W2 < 0.5$ for galaxy-like (Stern et al. 2012; Yan et al. 2013). The W1-W2 at E1 is 0.79 ± 0.02 , significantly lower than 0.93 ± 0.05 at the last three epochs (see bottom panel of Figure 1), indicating likely that it is experiencing an extra high energy input in addition to AGN at E1. Therefore, we think that the flux excess at E1 is not simply due to AGN variability.

K17 has presented UV-optical-IR light curves of PS1-10adi up to ~ 2200 days since the peak (see their Supplementary Figure 1). When we look through them carefully, it's worthwhile to find that there's a tiny yet notable hump at $\text{MJD} \approx 57,293$. For ease of convenience, we call the first major flare as the "primary outburst" and the second peak as "rebrightening". Interestingly, the rebrightening looks also occurs subsequently in W1 and W2, in which the W2 lags behind W1 by about half year. The W1 and W2 magnitudes have brightened by 0.12 ± 0.03 (4σ) and 0.08 ± 0.05 (1.6σ) at E6, while by 0.06 ± 0.04 (1.5σ) and 0.16 ± 0.04 (4σ) at E7, respectively.

3. EVAPORATION AND ECHO OF TORUS DUST

3.1. Infrared Echo of Torus Dust

TABLE 1
 WISE DATA

Epoch (1)	MJD (2)	W1m (3)	W2m (4)	W1 (5)	W2 (6)	W1-W2 (7)	$\log L_{W1}$ (8)	$\log L_{W2}$ (9)	T_{dust} (10)	$\log L_{\text{dust}}$ (11)
E1	55325	14.50 ± 0.01	13.71 ± 0.01	16.42 ± 0.02	16.83 ± 0.03	-0.41	42.9	42.4
E2	55505	13.29 ± 0.01	12.68 ± 0.01	13.64 ± 0.01	13.17 ± 0.03	0.47	44.1	43.9	1972	44.3
E3	56788	14.33 ± 0.02	13.28 ± 0.03	15.68 ± 0.02	14.39 ± 0.04	1.29	43.2	43.3	886	43.5
E4	56969	14.50 ± 0.04	13.48 ± 0.03	16.42 ± 0.04	15.50 ± 0.04	1.37	42.9	43.1	843	43.2
E5	57150	14.60 ± 0.03	13.65 ± 0.03	17.31 ± 0.03	16.09 ± 0.05	1.22	42.6	42.7	927	42.8
E6	57329	14.58 ± 0.02	13.69 ± 0.05	17.03 ± 0.03	16.60 ± 0.06	0.43	42.7	42.5	2114	43.0
E7	57517	14.63 ± 0.03	13.61 ± 0.03	17.75 ± 0.04	15.77 ± 0.05	1.98	42.4	42.8	620	43.1
Q	57881	14.70 ± 0.02	13.77 ± 0.03	0.93

NOTE. — Column (1): observational epochs. Column (2): median modified Julian Date. Column (3)-(4): median W1 and W2 magnitudes. Column (5)-(6): background-subtracted W1 and W2 magnitudes. Column (7): background-subtracted W1-W2 color. Column (8)-(9): background-subtracted W1 and W2 monochromatic luminosity. Column (10): dust temperature inferred from W1-W2 color assuming blackbody radiation. Column (11): the logarithmic integrated dust blackbody luminosity.

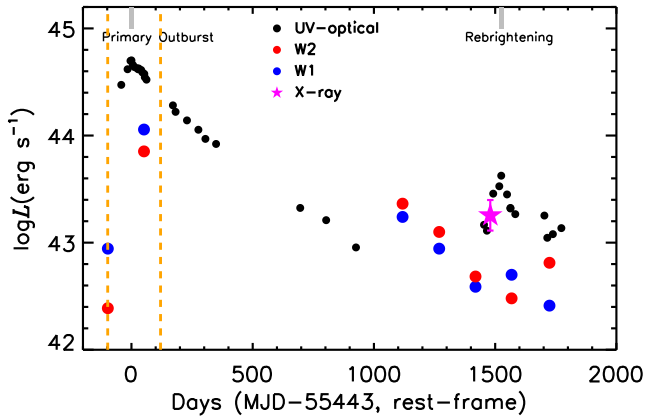


FIG. 2.— The luminosity evolution of PS1-10adi. The black, blue and red dots represent the UV-optical blackbody fitted luminosity, *WISE* W1 and W2 luminosity respectively. We have marked the peak time of the primary outburst and rebrightening. The X-rays detected during the rebrightening is plotted as a magenta five-pointed star. The region between the two orange dashed lines denotes the time when the torus dust is sublimating.

The IR flares detected in TDEs thus far are all successfully translated into dust echoes (Jiang et al. 2106, 2017; Dou et al. 2016, 2017; van Velzen et al. 2016). The dust, if there, in the vicinity of SMBHs will certainly absorb the primary emission of TDEs (soft X-ray, UV and optical) and reprocess them into IR, so we expect the flare in the IR would lag behind the optical (Lu et al. 2016). However, in some cases, the mid-IR variability could be detectable even earlier than the optical band and thus the echo interpretation is not so obvious. For example, we recently found a mid-IR flare that started ~ 11 days before the optical detection of a TDE candidate PS16dtm (Jiang et al. 2016). Interpreting the mid-IR flare as a dust echo requires close pre-existing dust with a high covering factor, which is fully qualified with the geometrically and optically thick torus in AGNs. The case in PS1-10adi looks even more extreme, in which the mid-IR brightening is detectable 118 (or rest-frame 98) days earlier than the optical discovery. Can it be explained by the scenario of PS16dtm as well?

The AGN property before the outburst is unfortunately missing due to lack of observations, yet can be supposed to be almost the same as the post-flare state. For the sake of an estimate, we have fitted the optical spectra at +1600 days (see Supplementary Figure 2 of K17) and obtained that the broad $H\alpha$ luminosity ($L_{H\alpha}$) is 8.8×10^{41} erg s^{-1} with a full width at half maximum (FWHM) of 3,676 km s^{-1} . By virtue of the empirical relation of M_{BH} in AGNs estimated from the lu-

minosity and FWHM of broad $H\alpha$ line (Greene & Ho 2005), the M_{BH} is $2.7 \times 10^7 M_{\text{BH}}$. Using the bolometric correction given by Greene & Ho 2007, the bolometric luminosity (L_{bol}) is $2.34 \times 10^{44} (L_{H\alpha}/10^{42})^{0.86} = 2.1 \times 10^{44}$ erg s^{-1} . The peak background-subtracted L_{bol} associated with the flare inferred from the UV-optical emission is $\sim 5 \times 10^{44}$ erg s^{-1} (see Figure 2), thus the total peak L_{bol} is $\sim 7 \times 10^{44}$ erg s^{-1} provided that all of the radiation is originated from the BH accretion.

In order to assess if the energy budget for the dust echo is reasonable, we have fitted the background-subtracted UV-optical-IR SEDs at different epochs using double-blackbody model, one for the original outburst emission dominating UV-optical band and the other for the reprocessed dust emission peaked in the IR (see an example in the top panel of Figure 3). We take the integrated luminosity of the blue component as the L_{bol} (see its evolution in Figure 2). Since there is no reliable detection of residual UV-optical emission at E1, a single blackbody is adopted and yields an ultra-high dust temperature of $\sim 10^7$ K. The value seems absolutely unreasonable probably because of a non-equilibrium condition, too simplified model and insensitivity to the slope of Rayleigh-Jeans tail for very high blackbody temperature. Therefore, we believe that the dust at E1 is sublimating in spite of the very uncertain dust temperature.

The double-blackbody fitting at E2 yields a dust temperature (T_{dust}) of $2,150 \pm 430$ K, that is consistent with the dust sublimation temperature within error. Assuming that the equilibrium T_{dust} of a dust grain with radius a at distance of R from the heating source is determined by the balance between the radiative heating by UV-optical photons and the thermal re-emission in the IR:

$$\frac{L_{\text{bol}}}{4\pi R^2} \pi a^2 = 4\pi a^2 \sigma T^4. \quad (1)$$

The calculated L_{bol} is 1.1×10^{45} erg s^{-1} given a dust distance $R = 52$ light days by the time lag to the optical peak. The value is slightly higher yet comparable to the observed peak L_{bol} (L_{peak}) of 7×10^{44} erg s^{-1} , providing valid evidence for the dust echo interpretation.

3.2. Evaporation of Torus Dust and the Fe II Emergence

The torus inner radius can be computed by the dust sublimation radius (R_{sub}) below (here we used the formula given in Namekata & Umemura 2016):

$$R_{\text{sub}} = 0.121 \text{ pc} \left(\frac{L_{\text{bol}}}{10^{45} \text{ erg s}^{-1}} \right)^{0.5} \left(\frac{T_{\text{sub}}}{1800 \text{ K}} \right)^{-2.804} \left(\frac{a}{0.1 \mu\text{m}} \right)^{-0.510} \quad (2)$$

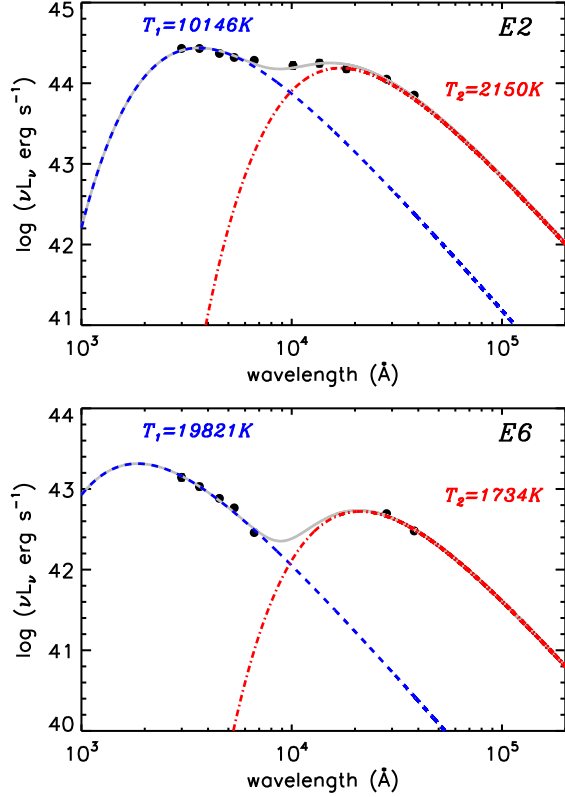


FIG. 3.— The background-subtracted SED of PS1-10adi at E2 (MJD \approx 55,505) and E6 (MJD \approx 57,323). The optical-NIR photometry is drawn from supplementary table 2 and table 3 of K17. We have tried to fit the SED using double-blackbody model, one for the UV-optical emission (blue dashed line) and the other for the dust emission (dot-dashed line).

The original torus inner radius is determined by the L_{bol} before the primary outburst, whose corresponding R_{sub} is 5.6×10^{-2} pc, that is 66 light days. As the luminosity of PS1-10adi increases, the illuminated dust in the inner region evaporates gradually, pushing the inner side of dusty torus outward. The calculation at the optical peak yields a new R_{sub} of 0.10 pc (\sim 120 light days), so the pre-existing dust located between 66 and 120 light days should have been evaporated.

The dust sublimation as a function of temperature can be estimated by

$$\frac{dm}{dt} = -\rho A \nu_0 \left(\frac{\mu}{\rho}\right)^{1/3} e^{-B/kT} \quad (3)$$

We adopt $\rho = 2.5 \text{ g cm}^{-3}$, $\nu_0 \simeq 10^{15} \text{ s}^{-1}$, $B/k = 7 \times 10^4 \text{ K}$, $\rho/\mu = 10^{23} \text{ cm}^{-3}$ following Equation 7 of Lu et al. 2016, which are representative values for refractory grains (Guhathakurta & Draine 1989; Waxman & Draine 2000). The A is the total illuminated dust area, that is $1.7 \times 10^{35} \text{ cm}^2$ at E2 ($A = L_{\text{dust}}/\sigma T^4$), giving a dust sublimation rate $dm/dt = 1.0 \times 10^{26} \text{ g s}^{-1}$. The precise mass of evaporated dust is difficult to acquire because of the poor sampling of the light curves. We hypothesize that the sublimation rate at E2 is an average value between -98 and +120 days (regions between the two orange dashed lines in Figure 2), the integrated evaporated dust is thus $\sim 1.9 \times 10^{33} \text{ g}$, that is around $1 M_{\odot}$.

Similar to the story told in PS16dtm (Jiang et al. 2017), metals originally reserved in the evaporated dust will enter into the gas and may be ionized, giving rise to metal lines,

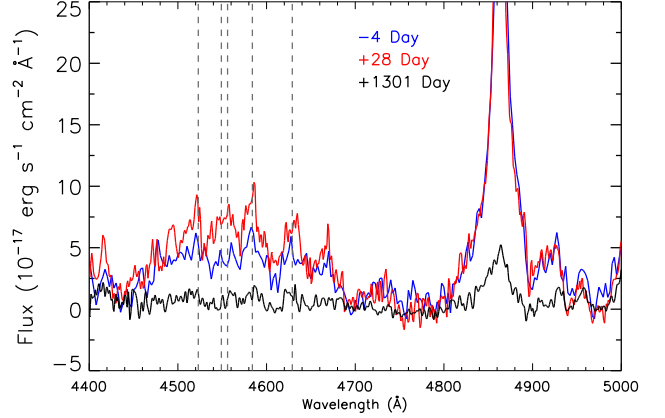


FIG. 4.— The variability of optical Fe II emission of PS1-10adi (data drawn from K17). Three spectra taken at -4 (blue), +28 (red) and +1301 days (black) respective to the optical peak are presented after the subtraction of continuum. The position of Fe II lines are marked as dashed grey lines. The Fe II intensity has strengthened at early stage (from -4 to 28 days) while faded over when the event ends (+1301 days).

such as Fe II multiplets observed in PS1-10adi (Figure 4, see also Supplementary Figure 2 in K17), making it resemble a classical narrow-line Seyfert 1 galaxy. If we believe that metals are mostly locked in the dust and the gas holds the solar metallicity, the gas mass should be higher than the dust mass by a factor of $\alpha \sim 50$. Supposing that the gas is distributed in the spherical region (outer radius $R_0 = 120$ light days) with a covering factor of f_c , the column density of the new broad-line region (BLR) can be calculated as below.

$$N_{\text{H}} = \frac{\alpha m_{\text{dust}}}{4\pi f_c R_0^2 m_{\text{H}}} \quad (4)$$

The derived N_{H} is $1.2 \times 10^{23} \text{ cm}^{-2}$, in which we have adopted the $f_c = 0.4$ (see §5.3). Both the gas mass and N_{H} of new BLR here are comparable with typical AGNs (Peterson 1997; Netzer 2013), indicating that they are likely sufficient to produce the observed Fe II strength even if the physical mechanisms are still not very clear to date. It is worthwhile to note that the Fe II multiplets have almost vanished after the outburst (see its +1301 days spectrum in Figure 4), agreeing well with the photoionization model.

Many previous studies show that the photoionization can not fully address the Fe II emission of AGNs (Collin & Joly 2000; Sigut & Pradhan 2003; Baldwin et al. 2004) yet collisional excitation might also act (e.g., Joly 1981; Véron-Cetty et al. 2006). This could be feasible in TDEs because the unbound debris ejected from the disrupted star may cause shocks by interacting with the gas and excite the iron. One needs to illustrate whether the time of collision is early enough to result in the instant presence of Fe II. The maximum escaping velocity of the unbound debris $v_{\text{max}} = (2GM_{\text{BH}}R_*/R_t^2)^{1/2} = 9 \times 10^3 \text{ km s}^{-1}$ in the case of one solar mass star disrupted by a $\sim 10^7 M_{\odot}$ BH, so the timescale of reaching the torus is $r_{\text{torus}}/v_{\text{max}} = 6 \text{ yr}$ given a r_{torus} of 66 light days. For the bound debris, although the circularization process is still not fully understood yet, several simulations show that the circularization timescale is in the range of several times to ~ 10 times the orbital period of the most bound debris (Bonnerot et al. 2016; Hayasaki et al. 2016). The period of the most bound debris can be estimated by $T_{\text{min}} = 2\pi GM_{\text{BH}}(-2\epsilon_{\text{min}})^{-3/2}$ in which $\epsilon_{\text{min}} = -GM_{\text{BH}}R_*/R_t^2$ is

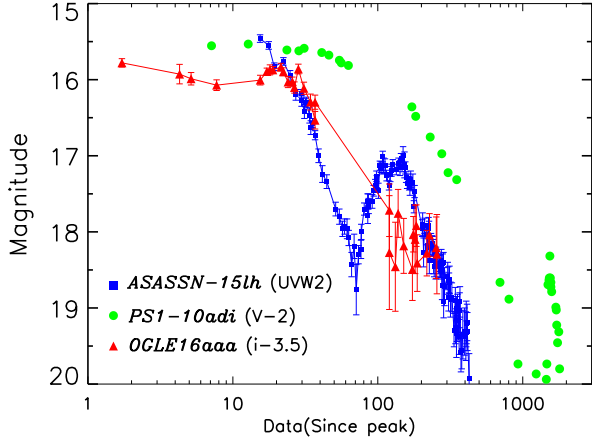


FIG. 5.— The comparison of the three TDE candidates with rebrightening-like light curves. Apart from the late-stage rebrightening of PS1-10adi (green dots), ASASSN-15lh presents a giant double-peaked light curve (blue squares, data from Godoy-Rivera et al. 2017) yet OGLE16aaa (red triangles, data from OGLE-IV Transient Detection System (<http://ogle.astrouw.edu.pl/ogle4/transients/2017a/transients.html>)) shows a slight rebrightening at earlier stage.

the lowest specific mechanical energy. The derived $T_{\min} \sim 0.6$ yr, meaning that the circularization timescale could be also as long as years yet with large uncertainties.

In brief, we surmise that the rapid emergence of prominent Fe II lines could be a universal characteristic of TDEs in AGNs, which will potentially promote us to understand the origin of Fe II emission in AGNs.

4. LATE-STAGE REBRIGHTENING

4.1. Late Accretion?

The rebrightening hump appeared in the UV-optical light curve is non-negligible while it has not been discussed in K17. As it happens, the similar hump is also present in the mid-IR light curve, with W1 band ahead of W2. Besides that, the X-ray emission has been first detected with a 0.3–10 keV luminosity of 2×10^{43} erg s⁻¹ during the rebrightening (see Supplementary Table 4 of K17). Unfortunately, the photons are too few to constrain whether it’s dominated by soft X-rays or not.

First, we attempt to naively understand the rebrightening as a late-stage accretion. The peak L_{bol} of the rebrightening is lower than the primary outburst by one order of magnitude, the time delay of dust emission relative to the rebrightening should be ~ 100 days as long as no dust newly formed. The fitted T_{dust} at E6 is 1.7×10^3 K and then it has dropped quickly to $\sim 6 \times 10^2$ K at E7. The mid-IR emission at E6 requires $L_{\text{bol}} \approx 1.7 \times 10^{45}$ erg s⁻¹ according to equation 1, that is two orders of magnitude higher than the observed L_{bol} at ~ 100 days before E6. One way may resolve the conflict is that the blackbody assumption for dust emission could be over-simplistic and the dust absorption efficiency ($Q_{\text{abs}} \propto \nu^\beta$) should be taken into account. The β value is quite uncertain: it approaches zero for very large grain (grey case); while for small grains, β strongly depends on the composition, i.e. $\simeq 2$ for graphite, $\simeq 1$ for silicate, and $\simeq -0.5$ for SiC. If we adopt $\beta = 2$ (see formula 8.16 in Kruegel 2003):

$$\frac{L_{\text{bol}}}{16\pi^2 R^2} \simeq 1.47 \times 10^{-6} a T^6, \quad (5)$$

we get $T_{\text{dust}} = 1.0 \times 10^3$ K, calling for L_{bol} of 1.3×10^{43} erg s⁻¹ for dust with MRN size distribution (Mathis et al. 1977), that is still comparable with the observation. However, it is hard to imagine that the dust properties responsible for E2 and E6 are so different. The other negative evidence stems from the concomitant X-ray emission, which is strangely absent in the early accretion but not in the late accretion. Therefore, we conclude that the late-stage accretion scheme is very unlikely.

4.2. Rebrightening in Other TDEs

We have noticed that among reported TDEs, ASASSN-15lh and OGLE16aaa also show a rebrightening characteristic in their UV-optical light curves (see Figure 5). In fact, it’s exactly the giant double-humped feature that motivated reconsideration of the nature of ASASSN-15lh, which was first claimed to be an unprecedentedly luminous SNe in view of its spectral resemblance to hydrogen-poor super-luminous SNe (SLSNe) at early stage (Dong et al. 2016). Together with several other lines of evidence by further monitoring (e.g., temperature evolution), ASASSN-15lh can be better understood as a TDE occurred in a spinning BH with mass of $3 \times 10^8 M_\odot$ (Leloudas et al. 2016; Krühler et al. 2018) rather than a SNe. Coincidentally, the X-ray emission hasn’t been detected in ASASSN-15lh either until the rebrightening, which is about 4 months after the primary peak (Margutti et al. 2017). Both the circularization (Guillochon & Ramirez-Ruiz 2015) and reprocessing (Metzger & Stone 2016) models have been suggested possible to address the intriguing UV-optical light curve (Leloudas et al. 2016). The rebrightening of OGLE16aaa is visible, yet much less obvious as ASASSN-15lh. Wyrzykowski et al. 2017 has tried to explain the variability as induced by a binary BH on a tight orbit or due to disc precession or circularization on a timescale of about a month. *Swift* observations taken around the same time of optical flare detected no X-ray emission. However, further *Swift* exposures at ~ 140 dates later enabled us to detect significant X-ray emission from this event, which then decayed and faded over a few months (Auchettl et al. 2017).

Both the rebrightening as well as associated X-ray onset in ASASSN-15lh and OGLE16aaa are similar to PS1-10adi, indicating plausibly a common and unified phenomenon in TDEs waiting to be understood. However, PS1-10adi is still somehow different from the other two. First, its occurring time of the rebrightening relative to the primary outburst is much later (see Figure 5), at some 1500 days when the TDE emission has almost disappeared. Second, the pc-scale gas and dust around the SMBH of PS1-10adi should be pretty ample, evidenced by the intense usual AGN activity and high dust covering factor revealed by the dust echo (see S5). In contrast, the nucleus of ASASSN-15lh and OGLE16aaa are relatively quiescent despite of weak AGN signatures (Krühler et al. 2018; Wyrzykowski et al. 2017).

4.3. Interaction between Debris or Outflow and Torus

The particularities of PS1-10adi encouraged us to come up with possible new mechanisms of the rebrightening. Could it be caused by the collision between the unbound stellar debris and the interstellar medium (ISM) at scale of AGN torus? The spread of specific orbital energy $\Delta\epsilon = GM_{\text{BH}}R_*/R_t^2$ is almost a constant for a large range of $\beta \equiv r_t/r_p$ (Stone et al. 2013; Tejada et al. 2017). The total orbital energy of unbound debris is $\Delta E < 0.5M_\odot \times 0.5\Delta\epsilon$. The interaction timescale for this collision is $t_{\text{intact}} \sim 0.5r_{\text{torus}}/0.5v_{\text{max}} = r_{\text{torus}}/v_{\text{max}} \sim 1500$

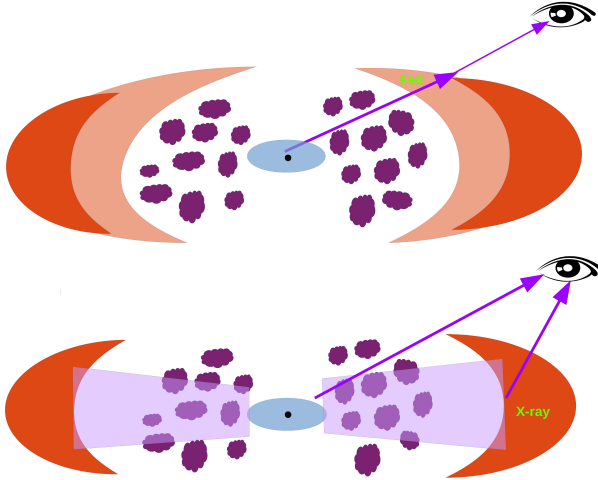


FIG. 6.— Schematic of the PS1-10adi model. In the standard AGN unification, SMBH (black solid circle), accretion disk (blue ellipse), BLR (aubergine clouds) and torus (orange tori) are distributed from inside to outside. Top panel: the central engine of PS1-10adi was partly obscured by torus yet largely exposed after the TDE due to the receding of torus. The metals released from the evaporated dust (light orange region) will give rise to the observed strong Fe II lines. Bottom panel: the high-speed outflow (denoted as light purple) launched from the accretion disk collides with the torus and produce the late-stage rebrightening and X-ray onset.

days. Therefore we can estimate the upper limit of rebrightening power assuming that all of the orbital energy can be transferred into the gas internal energy and radiate efficiently: $L_X(\text{max}) < \Delta E/t_{\text{intact}} = 1.5 \times 10^{42} \text{ ergs s}^{-1}$, which is one order of magnitude lower than observations. As a result, we argue that the rebrightening may not be due to the collision between the unbound debris and the torus.

Apart from the ejected debris, outflows launched by the TDE can also serve as a source of collision (see Figure 6 as an illustration). If that is the case, the observed outflow velocity can be estimated by $v_{\text{ej}} = r_{\text{torus}}/t_{\text{reb}} \sim 120/1500 * c = 2.4 \times 10^4 \text{ km s}^{-1}$. Outflows with such a kind of high velocity has been found in observations (e.g., Blanchard et al. 2017; Kara et al. 2018), and numerical simulations in which the outflow may be produced during the self-crossing process under the general relativistic precessing (e.g., Sądowski et al. 2016; Jiang et al. 2016), or from the final accretion disk with super-Eddington accretion rate (e.g., Dai et al. 2018). For example, in the simulation of Sądowski et al. 2016, about 10% of the star’s total mass can be transferred into outflow after the violent self-crossing, with outflowing velocity of $\sim 0.1c$, (yet we should stress that the simulated objects therein is 0.1 solar mass star tidal disrupted by a BH of $10^5 M_{\odot}$). Hence the total kinetic energy of this outflow is in the order of 10^{50} ergs. As a comparison, the integrated UV- optical bolometric light curve between 1500 and 2000 rest-frame days results in a total energy of $\sim 5 \times 10^{50}$ erg, which is on the same order of magnitude with the self-crossing outflow. In the torus interacting model, both the primary collisional and dust reprocessed emission are almost local, which can naturally address the high T_{dust} at the rebrightening stage. This is also supported by the time lag between the optical and IR rebrightening, which is shorter than the light travel time from BH to the new torus boundary (~ 100 days).

Last, we caution that besides the torus dust distributed in the equatorial plane around the accretion disk, dust elongated

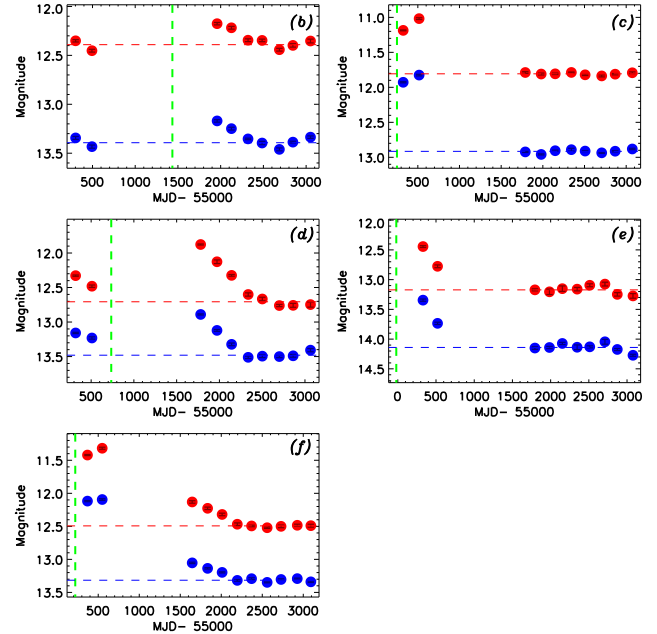


FIG. 7.— The WISE W1 (blue) and W2 (red) light curves of PS1-10adi analogs reported in K17. b-f: PS1-13jw, CSS100217, J094608, J094806 and J233454. The green dashed line marks the optical peak date.

in the polar direction has also been found in both type 1 and type 2 AGNs via recent mid-IR interferometry observations (Hönig et al. 2013) and SED fitting (Lyu & Rieke 2018). It’s suggested that a radiatively driven dusty wind, possibly launched in a puffed-up region of the inner hot part of the torus, is responsible for the polar dust (Hönig et al. 2012). The dusty wind is mostly optically thin and extends in the polar direction over parsecs or even tens of parsecs. On the other hand, the polar outflow is not inhibited inherently and has been tentatively reported in some broad absorption line quasars (e.g., Zhou et al. 2006). Therefore, the collision between the polar outflow and the polar dust can not be excluded completely to produce the observed rebrightening.

5. REVISITING THE NATURE OF PS1-10ADI AND ANALOGS

In previous sections, we have assumed that the nuclear transient in PS1-10adi is a TDE and have tried to understand all observations in the context of TDEs. However, as mentioned in K17, the case of extraordinary bright SNe occasionally exploded in the galactic nucleus is still impossible to disentangle from the TDE case up until then. In this section we will try to revisit the nature of PS1-10adi and other similar events with aid of mid-IR light curves.

5.1. Mid-IR Light Curves of PS1-10adi Analogs

Besides PS1-10adi, K17 has reported 5 other outbursts in the centers of active galaxies. They constitute the sample of highly-energetic nuclear transient events along with PS1-10adi. To understand their nature as a whole, we have retrieved their WISE and NEOWISE photometric data and presented the light curves in Figure 7. Significant mid-IR flare-like variability is visible for them all. As we already know the optical peak date of these events, we first estimated the background emission unassociated with the outbursts by averaging the magnitudes before or after the flares when the light curves maintain a stable level.

It’s interesting to note that a sustained MIR excess is present in J094608 before the optical flare. To exclude the probabil-

ity of spurious signal caused by a systematical bias between ALLWISE and NEOWISE-R data, we have performed aperture photometry on the time-resolved coadds of *WISE* images (Meisner et al. 2018). The excess ahead of the optical flare is proven to be real. It may be simply attributed to a higher dust covering factor than as the torus has receded to a further distance after the outburst, but it may be also reconciled by several alternative modes under the TDE scenario. Guillochon & Ramirez-Ruiz 2015 suggested that there is a delay between the flare and the disruption of the star of order years for BH mass of $10^7 M_{\odot}$. If the unbound debris collides with (torus) ISM, producing shocks and emitting UV/X-rays, it may lead to the enhanced IR emission before the primary outburst. This may be also a potential mechanism to address the early IR brightenings in PS16dtm (Jiang et al. 2017) and PS1-10adi (see §3). Other explanations, such as invoking stream collisions as a precursor to the main TDE flare (e.g., Bonnerot & Rossi 2018) or double TDEs induced by stellar binaries incident on SMBH binaries (Coughlin et al. 2018), are also possible. Owing to the deficiency of observational data before the event (e.g., X-rays), a thorough discussion of these possibilities is beyond of this work but could be tested in the future for TDEs with multiwavelength monitoring.

5.2. Infrared Luminosity Compared with Known Supernovas

The SNe scenario has been discussed by K17 in parallel with the TDE case. Spectroscopically, PS1-10adi bears similarity to type II SNe (SNe II, Schlegel 1990; Filippenko 1997), which is distinguished by relatively narrow emission lines and slowly declining light curves. The signatures of SNe II are not associated with the explosion itself, but rather with the interaction between ejecta and dense circumstellar medium (CSM) generally produced by pre-SN mass loss. SNe II have gained considerable attention over the past decade partly because they show a huge range in bolometric luminosity (e.g., Richardson et al. 2014; Li et al. 2011), among which the SLSNe are of greatest interest (e.g., Smith et al. 2007; Ofek et al. 2007; Gal-Yam 2012). It's firstly necessary to demonstrate why PS1-10adi and analogs prefer to be linked to AGNs if they are indeed SLSNe. One possible formation channel of these SLSNe has been proposed to be the runaway mergers of massive stars in dense and young stellar clusters, giving rise to very massive H-rich CSM (Portegies Zwart & van den Heuvel 2007), which seems feasible in high-density central regions of an active galaxy. The dense AGN environment can also provide suitable conditions for high ISM pressure as well as the photoionizing radiation to trap a large fraction of the mass lost from the progenitor (Mackey et al. 2014).

Could the SNe scenario also meet the mid-IR flare freshly revealed by the *WISE* light curve? Fox et al. 2011 have detected 10 out of 68 SNe II with late-time (>100 days) IR emission from a warm *Spitzer*/IRAC survey, holding a maximal IR luminosity of $10^8 \sim 10^9 L_{\odot}$, that is around 10^{42} erg s^{-1} . Statistically, the IR emission of SNe II are somewhat more luminous and more sustained than other types (e.g., type Ia), due to the heating of pre-existing dust by radiative shocks between the expanding SN shell and the dense wind of the progenitor (Fox et al. 2013; Tinyanont et al. 2016). Even so, the peak IR (W2 band) luminosity (L_{W2}) of PS1-10adi and analogous objects are uniformly higher than SNe II by at least one order of magnitude, exceeding 10^{43} erg s^{-1} . As a comparison, the L_{W2} maximum of the other AGN transient PS16dtm up

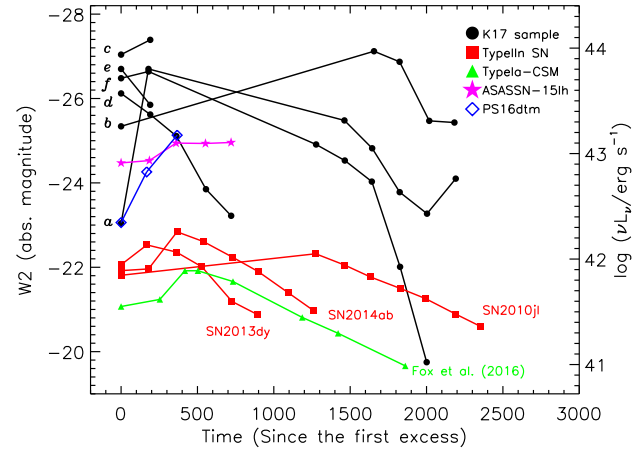


FIG. 8.— The *WISE* W2 ($4.6\mu\text{m}$) absolute magnitude (background-subtracted) of K17 sample and SNe with prominent mid-IR excesses. a-f: PS1-10adi, PS1-13jw, CSS100217, J094806, J094608 and J233454, namely the six objects listed in the supplementary table 1 of K17. The Type-II SNe are plotted in red squares and Type Ia-CSN SNe are shown as green triangles (Fox et al. 2016). We have also overplotted ASASSN-15lh (magenta star) and PS16dtm (blue diamonds) for comparison.

to 2017 July (latest public epoch) is also above 10^{43} erg s^{-1} (Jiang et al. 2017) already. We caution that previous *Spitzer* follow-ups (Fox et al. 2011) may have missed the early IR emission, so then we have subsequently checked the *WISE* light curves of all SNe II exploded during 2009 and 2016 from the open supernova catalog⁵ (Guillochon et al. 2017). Among them, the most IR luminous ones (e.g., SN2010jl, SN2013dy, SN2014ab) show no higher luminosity and still possess $L_{W2} \sim 10^{42}$ erg s^{-1} (see Figure 8). As we mentioned in §4.2, the controversial event ASASSN-15lh was discovered as a historical SLSNe at first while more observational facts later favour the TDE scenario. A mid-IR flare after the giant optical outburst has also been detected in ASASSN-15lh by *WISE* with peak $L_{W2} \sim 10^{43}$ erg s^{-1} , making it stand out from SNe despite slightly lower than PS1-10adi. In one word, the IR luminosity of PS1-10adi and analogs are significantly higher than known certified SNe II as well as any other types of SNe to our knowledge.

5.3. Dust Covering Factor: Consistent with AGN Torus

The extremely high IR luminosity of PS1-10adi can not reconcile with SNe, but seems fairly practical for TDEs in AGNs, in which the dusty torus around the BH will unavoidably absorb the TDE emission and reprocess them into the IR. To depict the dust content around PS1-10adi more quantitatively, we try to calculate its dust covering factor (f_{dust}), namely the fraction of the sky obscured by dust when seen from the central source. The idea is very straightforward that the original UV-optical photons towards the dust region will be entirely absorbed and re-emitted in the IR. Therefore, the ratio between energy radiated through dust reprocessing (E_{dust}) and total energy initially released by the event (E_{rad}) can be used to indicate f_{dust} (see also van Velzen et al. 2016). K17 has obtained a E_{rad} of $\sim 2.3 \times 10^{52}$ erg by integrating the UV-optical blackbody emission and taking into consideration of the early UV excess and missing rise-time contribution. Unfortunately, the precise calculation of E_{dust} is hindered by the sparse sampling and the 3-year-gap of the mid-IR

⁵ <https://sne.space/>

light curve. As an acceptable alternative, we have calculated the E_{dust} basing on the piecewise linear luminosity evolution, yielding a value of 1.0×10^{52} erg. The derived f_{dust} of PS1-10adi is thus ~ 0.4 , that is broadly consistent with AGNs estimated by other methods, such as fitting torus component to the SEDs of AGNs (e.g., Fritz et al. 2006; Mor et al. 2009; Roseboom et al. 2013). We have subsequently computed the f_{dust} for the left 5 events in K17 using the same approach and obtained comparable values.

The high f_{dust} of PS1-10adi is a natural consequence of AGNs, which is automatically satisfied in the TDE case as it happens in the accretion disk scale encircled by the torus. Core-collapse SNe have been believed to be one of the major production sites of cosmic dust grains (see a recent review by Sarangi et al. 2018), either by ejecting metal-rich materials into space for dust condensation or through the interaction between the ejecta and dense CSM. However, the amount of dust produced by an individual SNe is very limited and hard to manifest the SNe as a such high covering factor. The only conceivable SNe likelihood remained to be a SLSNe exploded inner or exactly in the torus (e.g., Assef et al. 2018). In the meantime, the torus or AGN gas may also provide the dense CSM that is thought to be needed to make the SNe super-luminous. The SNe scheme can not be ruled out completely with the caveat that the SNe explosion within the torus scale hasn't been well demonstrated.

We do not expect that the mid-IR echoes have the function to definitely diagnose the nature of PS1-10adi and analogs, but they indeed confine the outburst location to be no larger than the torus scale confidently. It's not trivial to differentiate TDEs and SNe with existing information and our current knowledge. Some other studies have even invoked peculiar AGN processes to generate these intense nuclear flares of Seyfert galaxies. For instance, the interaction between BH disk winds and BLR clouds is proposed to reproduce the observed luminosity and timescale (Moriya et al. 2017). In fact, a high-amplitude AGN variability could be misidentified as TDE or vice versa (e.g., Merloni et al. 2015; Saxton et al. 2018). In this way, the ionizing continuum and mid-IR echoes may be the least informative aspect of the transient, and other identifying signatures (e.g., chemical abundance ratio, Yang et al. 2017) are needed.

6. SUMMARY

The investigation of TDEs in AGNs has become more and more realizable thanks to the rapid development of time-domain astronomy nowadays. Continuing with our first dust echo case study on PS16dtm (Jiang et al. 2017), which is a TDE occurring in a Seyfert 1 host found by Pan-STARRS, we have next turned our attention to the other event PS1-10adi (K17) discovered by the same survey. The outburst of PS1-10adi happens much earlier than PS16dtm and thus yields a more complete light curve, that will provide us an excellent opportunity to understand TDEs in AGNs.

The mid-IR echoes appeared in both events display some distinctive characteristics by comparing with previous TDEs in quiescent galaxies. The complete understanding of these two events is beyond this work, yet their unusual behaviors can be largely attributed to a pre-existing dusty torus in AGNs but absent in quiescent galaxies. First, the mid-IR flares are detectable even earlier than the optical ones. The dust temperature naively fitted by blackbody emission in the early stage is higher than the dust sublimation temperature, indicating strongly on-going dust evaporation. We infer that it's the torus

dust around the BH that have (partially) obscured and weakened the optical emission, which has been conversely transferred to the IR emission. Along with the rising of the TDE bolometric luminosity, the inner radius of the torus receded until the peak luminosity. During this process, the metals originally contained in the dust will be delivered to the gas and give rise to the prominent Fe II multiplets seen in PS16dtm and PS1-10adi. The Fe II lines of PS1-10adi have faded over when the outburst ends, supporting strongly the photoionizing mechanism, although the collisional excitation may also act, triggered by the interaction between the unbound stellar debris with the torus gas in the TDE scenario.

The other intriguing feature of PS1-10adi is the late-stage UV-optical rebrightening at ~ 1500 rest-frame days after the primary outburst. The peak luminosity of the hump is $\sim 5 \times 10^{43}$ erg s^{-1} , that is two orders of magnitude lower than the primary peak. In agreement with most other optical TDEs, the X-rays hasn't been detected in the early stage (Auchettl et al. 2017). Interestingly, the *Swift* observation triggered during the rebrightening has captured the X-ray emission. In addition, there also exists a mid-IR rebrightening immediately after the the optical one. The late-stage accretion possibility is disfavoured by the ultra-high T_{dust} and X-ray emerging. We have also noticed that at least two other reported TDEs (ASASSN-15lh and OGLE16aaa) show somewhat similar behavior yet the rebrightening takes place at much earlier stage. Unlike the reprocessing or circularization model suggested in ASASSN-15lh, we have proposed a new mechanism responsible for the rebrightening inspired by the fact of AGN phase before PS1-10adi occurs. In this scenario, the collision between the high-speed outflow and the torus has resulted in the UV-optical rebrightening and X-ray onset. We suspect that it may be a universal phenomenon for the TDEs in AGNs. Further follow-ups of PS16dtm and more other events can help us confirm the idea or not.

The mid-IR light curves analyzed in this work can also help us understand the nature of these highly energetic transient events in the centers of active galaxies. The peak IR luminosities of PS1-10adi and analogs are more than 10 times higher than all known IR-luminous SNe, but could be rare SNe exploded in the torus. Moreover, their IR luminosity is also much higher than normal TDEs in quiescent galaxies (e.g., Jiang et al. 2016; van Velzen et al. 2016). It can be easily understood as the dusty torus effect, which solely acts in AGNs. The torus has obscured the central engine of PS1-10adi with a covering factor of ~ 0.4 and radiatively transferred a large fraction of high energy photons to the IR band.

Tori is an essential ingredient in the AGN unification model to explain various observational characteristics exhibited in different types of AGNs although its attributes are still far away from clarity. TDEs in AGNs may enable us to probe the torus from a novel perspective. The dust echo of the torus will respond to the tidal disruption radiation as an outstanding mid-IR flare, which is presumably even remarkable than the optical flare. The time delay of the flare in the mid-IR to the optical is an expression of the torus physical scale and the total radiated energy in the IR can be used to measure the dust covering factor of AGN. Similar phenomenon has also been reported in the other sorts of systems undergoing dramatic change of accretion rate, namely changing-look AGNs in which the AGN type has transited from type 1 to type 2 or vice versa (Sheng et al. 2017; 2018 in preparation). Moreover, the interaction between the high-speed outflow

and ISM may also give useful insights into the torus information. The new approach demands timely trigger of mid-IR monitoring (e.g., *Spitzer*) of the TDE candidates found in AGNs by X-ray or optical band. On the other hand, the mid-IR flares identified from surveys like *WISE* (Jiang et al. in preparation) also deserve prompt follow-ups in other bands (e.g., X-rays). The complete coverage of all events at each band is too expensive and unrealistic, yet could be achieved by certain well-defined projects at the upcoming golden era of time-domain astronomy.

We thank for the anonymous referee for many constructive comments and suggestions. We thank Dr. Erkki Kankare for providing us the optical spectra data of PS1-10adi. This work is supported by the National Basic Research Pro-

gram of China (grant No. 2015CB857005), NSFC (NSFC-116203021, NSFC-11703022, NSFC-11833007), Joint Research Fund in Astronomy (U1431229, U1731104) under cooperative agreement between the NSFC and the CAS, Anhui Provincial Natural Science Foundation and the Fundamental Research Funds for the Central Universities. This research makes use of data products from the *Wide-field Infrared Survey Explorer*, which is a joint project of the University of California, Los Angeles, and the Jet Propulsion Laboratory/California Institute of Technology, funded by the National Aeronautics and Space Administration. This research also makes use of data products from *NEOWISE-R*, which is a project of the Jet Propulsion Laboratory/California Institute of Technology, funded by the Planetary Science Division of the National Aeronautics and Space Administration.

REFERENCES

- Assef, R. J., Prieto, J. L., Stern, D., et al. 2018, *ApJ*, 866, 26
 Auchettl, K., Guillochon, J., & Ramirez-Ruiz, E. 2017, *ApJ*, 838, 149
 Baldwin, J. A., Ferland, G. J., Korista, K. T., Hamann, F., & LaCluyzé, A. 2004, *ApJ*, 615, 610
 Blanchard, P. K., Nicholl, M., Berger, E., et al. 2017, *ApJ*, 843, 106
 Bogdán, Á., & Goulding, A. D. 2015, *ApJ*, 800, 124
 Bonnerot, C., Rossi, E. M., Lodato, G., & Price, D. J. 2016, *MNRAS*, 455, 2253
 Bonnerot, C., & Rossi, E. M. 2018, arXiv:1805.09329
 Chen, M. C., Broadhurst, T., Lim, J., et al. 2018, *ApJ*, 863, 135
 Collin, S., & Joly, M. 2000, *New Astronomy*, 44, 531
 Coughlin, E. R., Darbha, S., Kasen, D., & Quataert, E. 2018, *ApJ*, 863, L24
 Dai, L., McKinney, J. C., Roth, N., Ramirez-Ruiz, E., & Miller, M. C. 2018, *ApJ*, 859, L20
 Dong, S., Shappee, B. J., Prieto, J. L., et al. 2016, *Science*, 351, 257
 Dou, L., Wang, T., Jiang, N., et al. 2016, *ApJ*, 832, 188
 Dou, L., Wang, T., Yan, L., et al. 2017, *ApJ*, 841, L8
 Filippenko, A. V. 1997, *ARA&A*, 35, 309
 Fox, O. D., Chevalier, R. A., Skrutskie, M. F., et al. 2011, *ApJ*, 741, 7
 Fox, O. D., Filippenko, A. V., Skrutskie, M. F., et al. 2013, *AJ*, 146, 2
 Fox, O. D., Johansson, J., Kasliwal, M., et al. 2016, *ApJ*, 816, L13
 Fritz, J., Franceschini, A., & Hatziminaoglou, E. 2006, *MNRAS*, 366, 767
 Gal-Yam, A. 2012, *Science*, 337, 927
 Godoy-Rivera, D., Stanek, K. Z., Kochanek, C. S., et al. 2017, *MNRAS*, 466, 1428
 Greene, J. E., & Ho, L. C. 2005, *ApJ*, 630, 122
 Greene, J. E., & Ho, L. C. 2007, *ApJ*, 670, 92
 Guhathakurta, P., & Draine, B. T. 1989, *ApJ*, 345, 230
 Guillochon, J., Manukian, H., & Ramirez-Ruiz, E. 2014, *ApJ*, 783, 23
 Guillochon, J., & Ramirez-Ruiz, E. 2015, *ApJ*, 809, 166
 Guillochon, J., Parrent, J., Kelley, L. Z., & Margutti, R. 2017, *ApJ*, 835, 64
 Hayasaki, K., Stone, N., & Loeb, A. 2016, *MNRAS*, 461, 3760
 Heckman, T. M., & Best, P. N. 2014, *ARA&A*, 52, 589
 Hezaveh, Y. D., Marshall, P. J., & Blandford, R. D. 2015, *ApJ*, 799, L22
 Hills, J. G. 1975, *Nature*, 254, 295
 Hönig, S. F., Kishimoto, M., Antonucci, R., et al. 2012, *ApJ*, 755, 149
 Hönig, S. F., Kishimoto, M., Tristram, K. R. W., et al. 2013, *ApJ*, 771, 87
 Jahnke, K., & Macciò, A. V. 2011, *ApJ*, 734, 92
 Jiang, N., Zhou, H.-Y., Ho, L. C., et al. 2012, *ApJ*, 759, L31
 Jiang, N., Dou, L., Wang, T., et al. 2016, *ApJ*, 828, L14
 Jiang, N., Wang, T., Yan, L., et al. 2017, *ApJ*, 850, 63
 Jiang, Y.-F., Guillochon, J., & Loeb, A. 2016, *ApJ*, 830, 125
 Joly, M. 1981, *A&A*, 102, 321
 Karas, V., & Šubr, L. 2007, *A&A*, 470, 11
 Kankare, E., Kotak, R., Mattila, S., et al. 2017, *Nature Astronomy*, 1, 865 (K17)
 Kara, E., Dai, L., Reynolds, C. S., & Kallman, T. 2018, *MNRAS*, 474, 3593
 Komossa, S. 2015, *Journal of High Energy Astrophysics*, 7, 148
 Kormendy, J., & Ho, L. C. 2013, *ARA&A*, 51, 511
 Kruegel, E. 2003, *The physics of interstellar dust, by Endrik Kruegel. IoP Series in astronomy and astrophysics*, ISBN 0750308613. Bristol, UK: The Institute of Physics, 2003.,
 Krühler, T., Fraser, M., Leloudas, G., et al. 2018, *A&A*, 610, A14
 Leloudas, G., Fraser, M., Stone, N. C., et al. 2016, *Nature Astronomy*, 1, 0002
 Li, W., Leaman, J., Chornock, R., et al. 2011, *MNRAS*, 412, 1441
 Lu, W., Kumar, P., & Evans, N. J. 2016, *MNRAS*, 458, 575
 Lyu, J., & Rieke, G. H. 2018, *ApJ*, 866, 92
 Mackey, J., Mohamed, S., Gvaramadze, V. V., et al. 2014, *Nature*, 512, 282
 Mainzer, A., Bauer, J., Cutri, R. M., et al. 2014, *ApJ*, 792, 30
 Mao, S., Witt, H. J., & Koopmans, L. V. E. 2001, *MNRAS*, 323, 301
 Margutti, R., Metzger, B. D., Chornock, R., et al. 2017, *ApJ*, 836, 25
 Mathis, J. S., Ruml, W., & Nordsieck, K. H. 1977, *ApJ*, 217, 425
 Meisner, A. M., Lang, D., & Schlegel, D. J. 2018, *AJ*, 156, 69
 Merloni, A., Dwelly, T., Salvato, M., et al. 2015, *MNRAS*, 452, 69
 Metzger, B. D., & Stone, N. C. 2016, *MNRAS*, 461, 948
 Mor, R., Netzer, H., & Elitzur, M. 2009, *ApJ*, 705, 298
 Moriya, T. J., Tanaka, M., Morokuma, T., & Ohsuga, K. 2017, *ApJ*, 843, L19
 Namekata, D., & Umemura, M. 2016, *MNRAS*, 460, 980
 Netzer, H. 2013, *The Physics and Evolution of Active Galactic Nuclei*, by Hagai Netzer, Cambridge, UK: Cambridge University Press, 2013,
 Netzer, H. 2015, *ARA&A*, 53, 365
 Ofek, E. O., Cameron, P. B., Kasliwal, M. M., et al. 2007, *ApJ*, 659, L13
 Ostriker, J. P. 2000, *Physical Review Letters*, 84, 5258
 Peng, C. Y. 2007, *ApJ*, 671, 1098
 Peterson, B. M. 1997, *An introduction to active galactic nuclei*, Publisher: Cambridge, New York Cambridge University Press, 1997 Physical description xvi, 238 p. ISBN 0521473489,
 Phinney, E. S. 1989, *The Center of the Galaxy*, 136, 543
 Portegies Zwart, S. F., & van den Heuvel, E. P. J. 2007, *Nature*, 450, 388
 Rees, M. J. 1988, *Nature*, 333, 523
 Richardson, D., Jenkins, R. L., III, Wright, J., & Maddox, L. 2014, *AJ*, 147, 118
 Roseboom, I. G., Lawrence, A., Elvis, M., et al. 2013, *MNRAS*, 429, 1494
 Sądowski, A., Tejeda, E., Gafton, E., Rossow, S., & Abarca, D. 2016, *MNRAS*, 458, 4250
 Sarangi, A., Matsuura, M., & Micelotta, E. R. 2018, *Space Sci. Rev.*, 214, 63
 Saxton, C. J., Perets, H. B., & Baskin, A. 2018, *MNRAS*, 474, 3307
 Schlegel, E. M. 1990, *MNRAS*, 244, 269
 Smith, N., Li, W., Foley, R. J., et al. 2007, *ApJ*, 666, 1116
 Sheng, Z., Wang, T., Jiang, N., et al. 2017, *ApJ*, 846, L7
 Sigut, T. A. A., & Pradhan, A. K. 2003, *ApJS*, 145, 15
 Stern, D., Assef, R. J., Benford, D. J., et al. 2012, *ApJ*, 753, 30
 Stone, N., Sari, R., Loeb, A., 2013, *MNRAS*, 435, 1809
 Stone, N. C., & Metzger, B. D. 2016, *MNRAS*, 455, 859
 Tejeda, E., Gafton, E., Rossow, S., & Miller, J. C., 2017, *MNRAS*, 469, 4483
 Tinyanont, S., Kasliwal, M. M., Fox, O. D., et al. 2016, *ApJ*, 833, 231
 van Velzen, S., Farrar, G. R., Gezari, S., et al. 2011, *ApJ*, 741, 73
 van Velzen, S., Mendez, A. J., Krolik, J. H., & Gorjian, V. 2016, *ApJ*, 829, 19
 Véron-Cetty, M.-P., Joly, M., Véron, P., et al. 2006, *A&A*, 451, 851
 Wang, J., & Merritt, D. 2004, *ApJ*, 600, 149
 Wang, T., Yan, L., Dou, L., et al. 2018, *MNRAS*, 477, 2943
 Waxman, E., & Draine, B. T. 2000, *ApJ*, 537, 796
 Wright, E. L., Eisenhardt, P. R. M., Mainzer, A. K., et al. 2010, *AJ*, 140, 1868-1881

Wyrzykowski, Ł., Zieliński, M., Kostrzewa-Rutkowska, Z., et al. 2017, MNRAS, 465, L114
Yan, L., Donoso, E., Tsai, C.-W., et al. 2013, AJ, 145, 55

Yang, C., Wang, T., Ferland, G. J., et al. 2017, ApJ, 846, 150
Zhao, H., Haehnelt, M. G., & Rees, M. J. 2002, NewA, 7, 385
Zhou, H., Wang, T., Wang, H., et al. 2006, ApJ, 639, 716